Supporting information

A Fast Charge/Discharge and Wide-Temperature Battery with a Germanium Oxide Layer on a Ti_3C_2 MXene Matrix as Anode

Mingwei Shang, Xi Chen, Bangxing Li and Junjie Niu*

Department of Materials Science and Engineering, CEAS, University of Wisconsin-Milwaukee, Milwaukee, WI 53211, USA

*Email: niu@uwm.edu

This file includes:

Figures S1 to S8 with legends

Tables S1 to S3

Calculation of the theoretical capacity of GeO_x

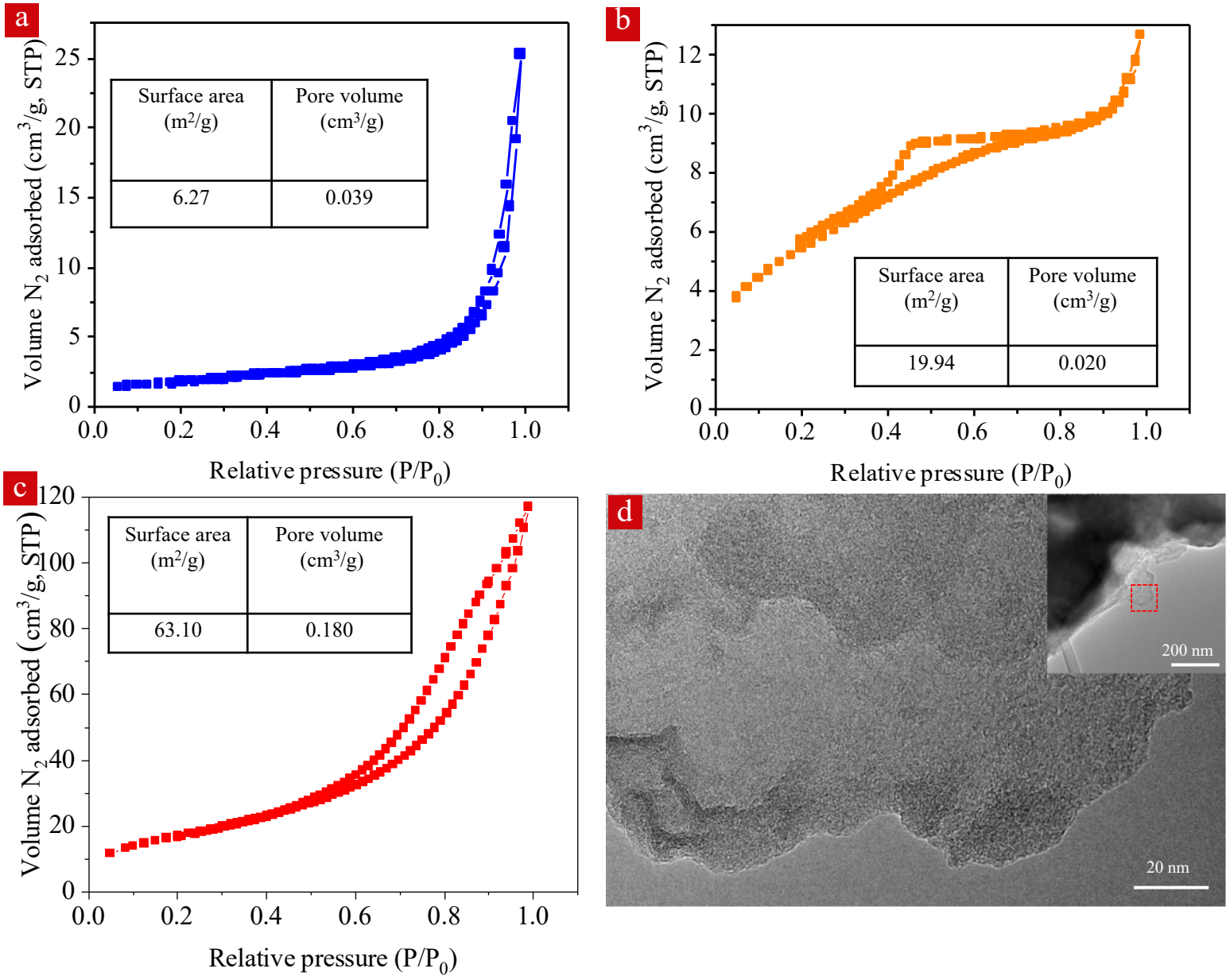

Figure S1. **Surface analysis of the samples.** Nitrogen sorption-desorption isotherms of (a) MXene, (b) GeO_x and (c) GeO_x@MXene. The insets are the corresponding surface area and pore volume. (d) TEM images of GeO_x@MXene.

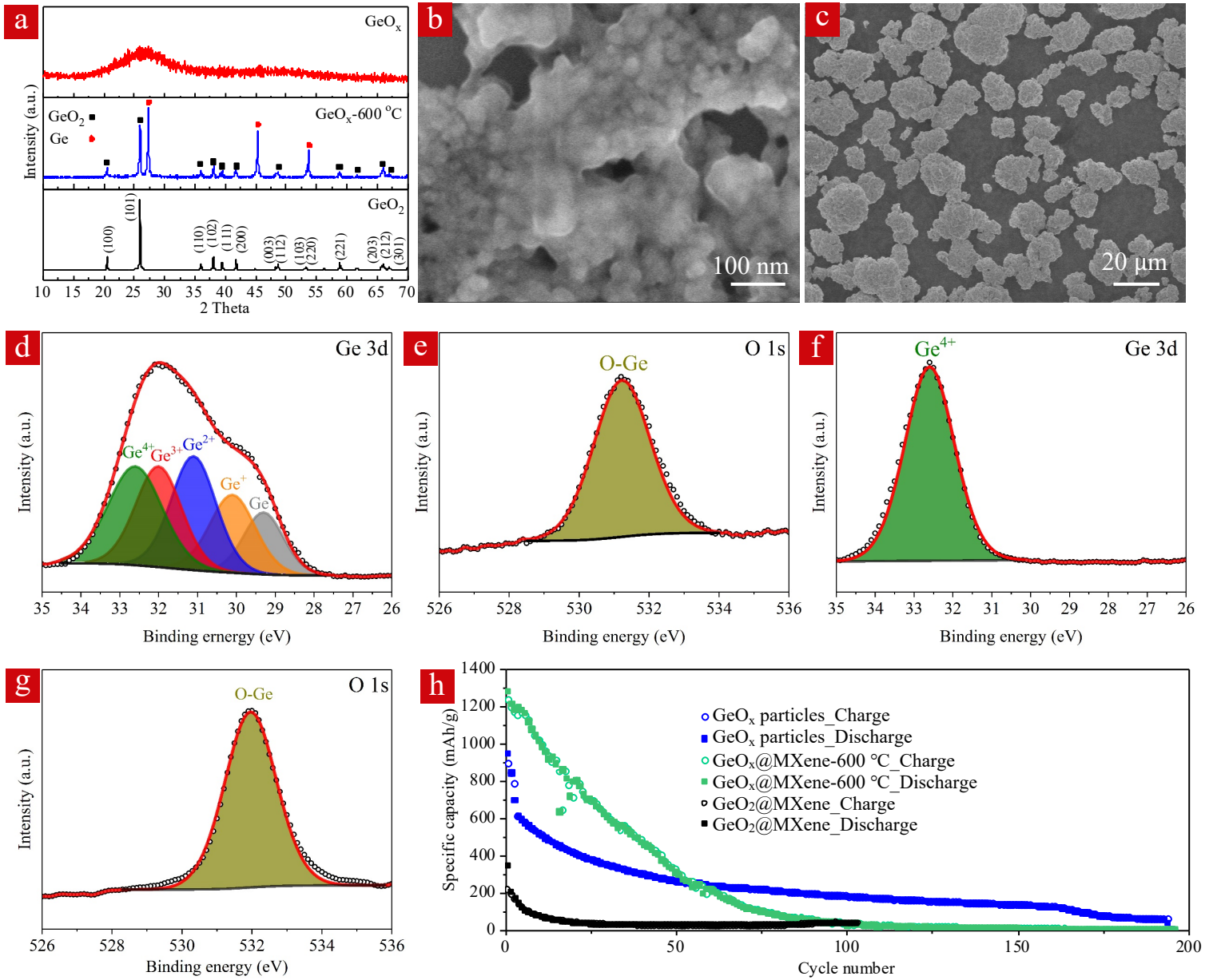

Figure S2. Structure and performance comparison with different materials. (a) XRD patterns of commercial GeO_2 and synthesized GeO_x particles before and after heating at 600 °C in argon. SEM images of (b) the synthesized GeO_x particles and (c) commercial GeO_2 powders. XPS analysis of (d) Ge 3d and (e) O 1s of GeO_x particles, (f) Ge 3d and (g) O 1s of commercial GeO_2 powders. (h) Battery cycling performance with GeO_x, GeO_x@MXene-600 °C and GeO_2@MXene (39.9 wt% GeO_2 mixed with MXene) as anode at 0.5 C and active material loading of 1.0 mg/cm^2, respectively.

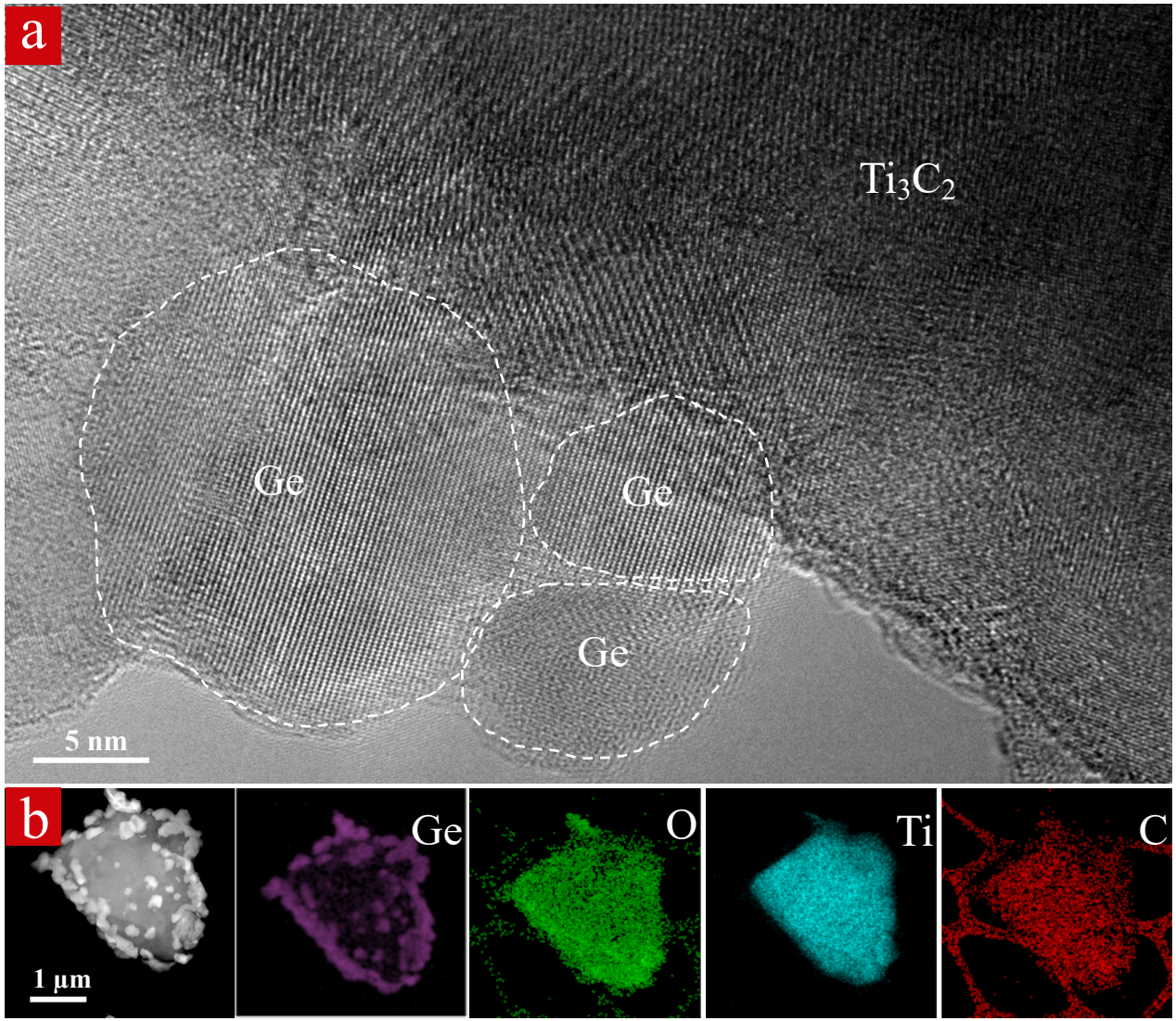

Figure S3. Morphology and chemical composition of GeO_x@MXene-600 ℃. (a) High-resolution TEM image and (b) EDS element mappings of Ge, Ti, C and O of the GeO_x@MXene-600 ℃.

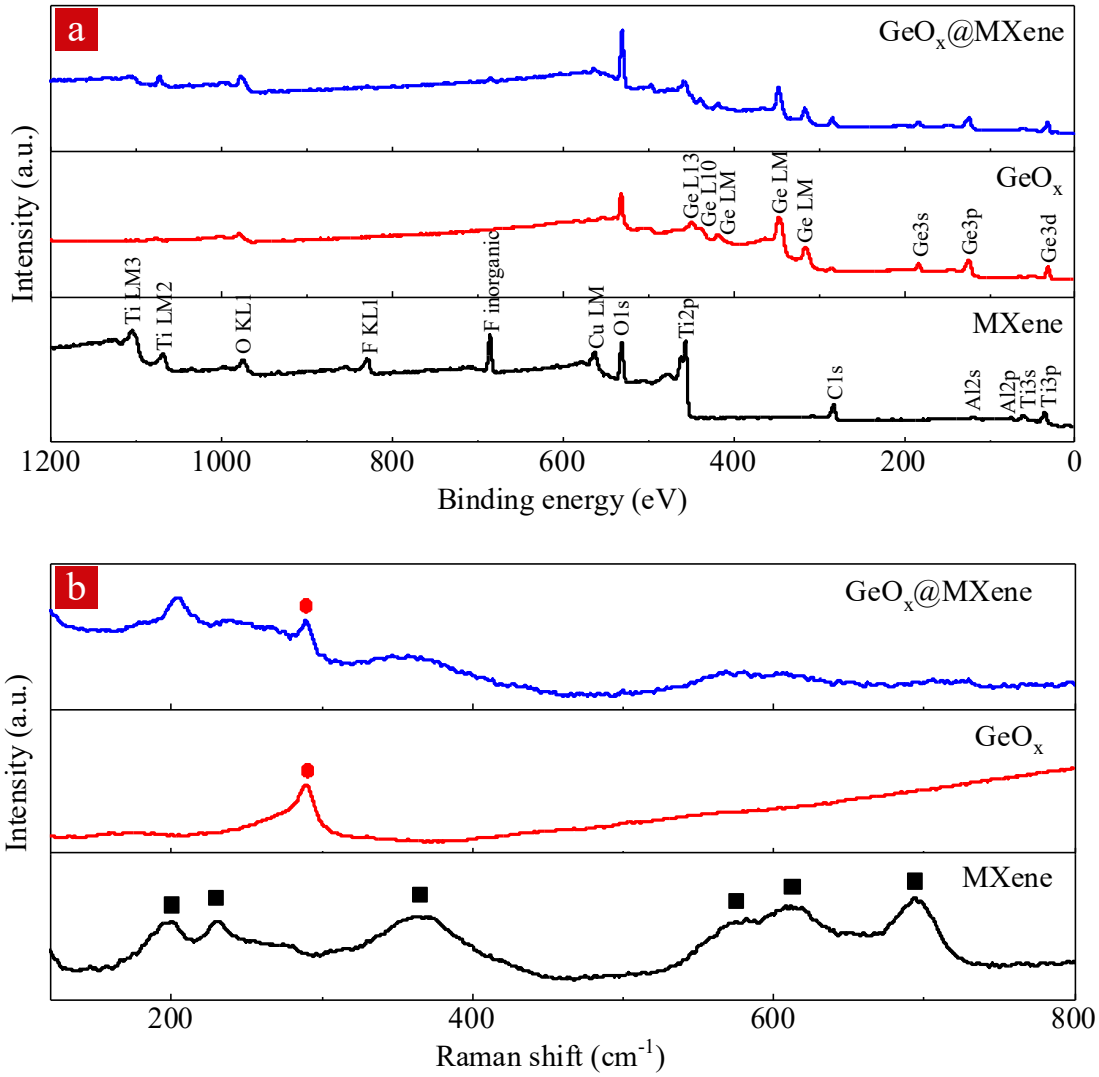

Figure S4. Spectroscopy analysis of the samples. (a) XPS survey and (b) Raman spectra of GeO_x@MXene, GeO_x, and MXene, respectively.

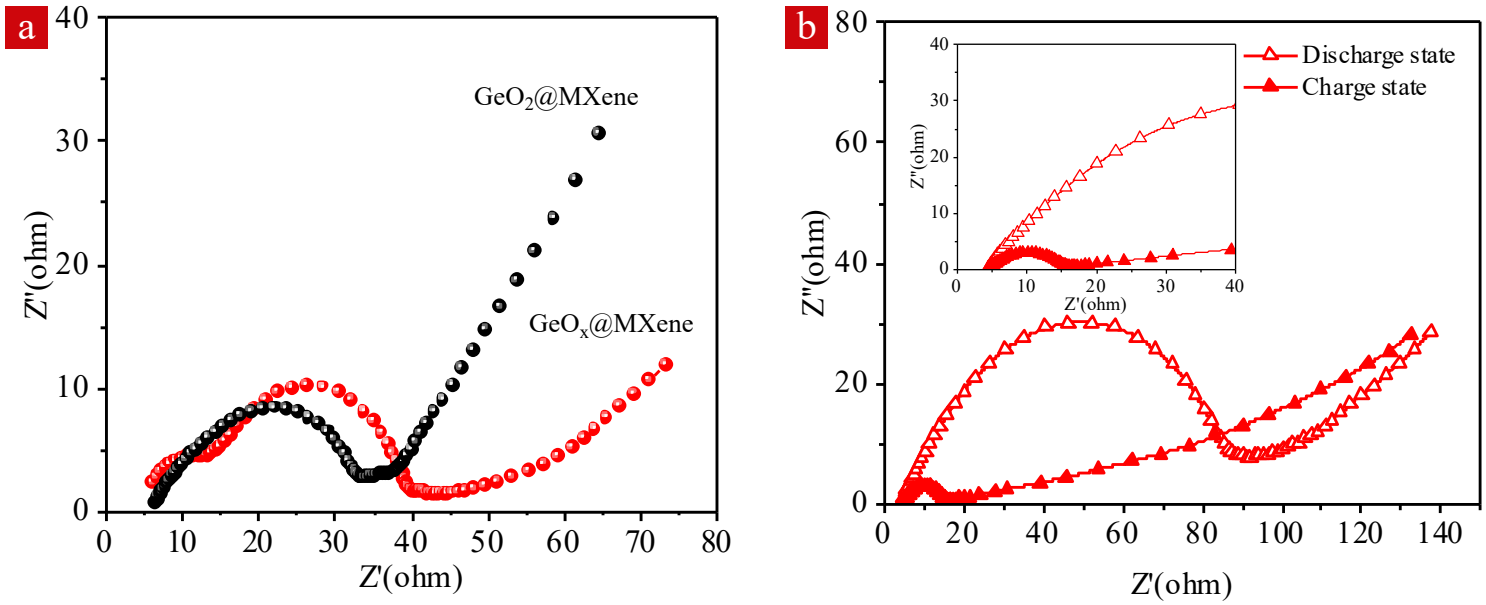

Figure S5. EIS results of the battery upon cycling. Nyquist plots of (a) GeO_x@MXene and GeO_2@MXene before cycling, and (b) GeO_x@MXene at charge/discharge states: stop at 1.5 V for charge; stop at 0.01 V for discharge.

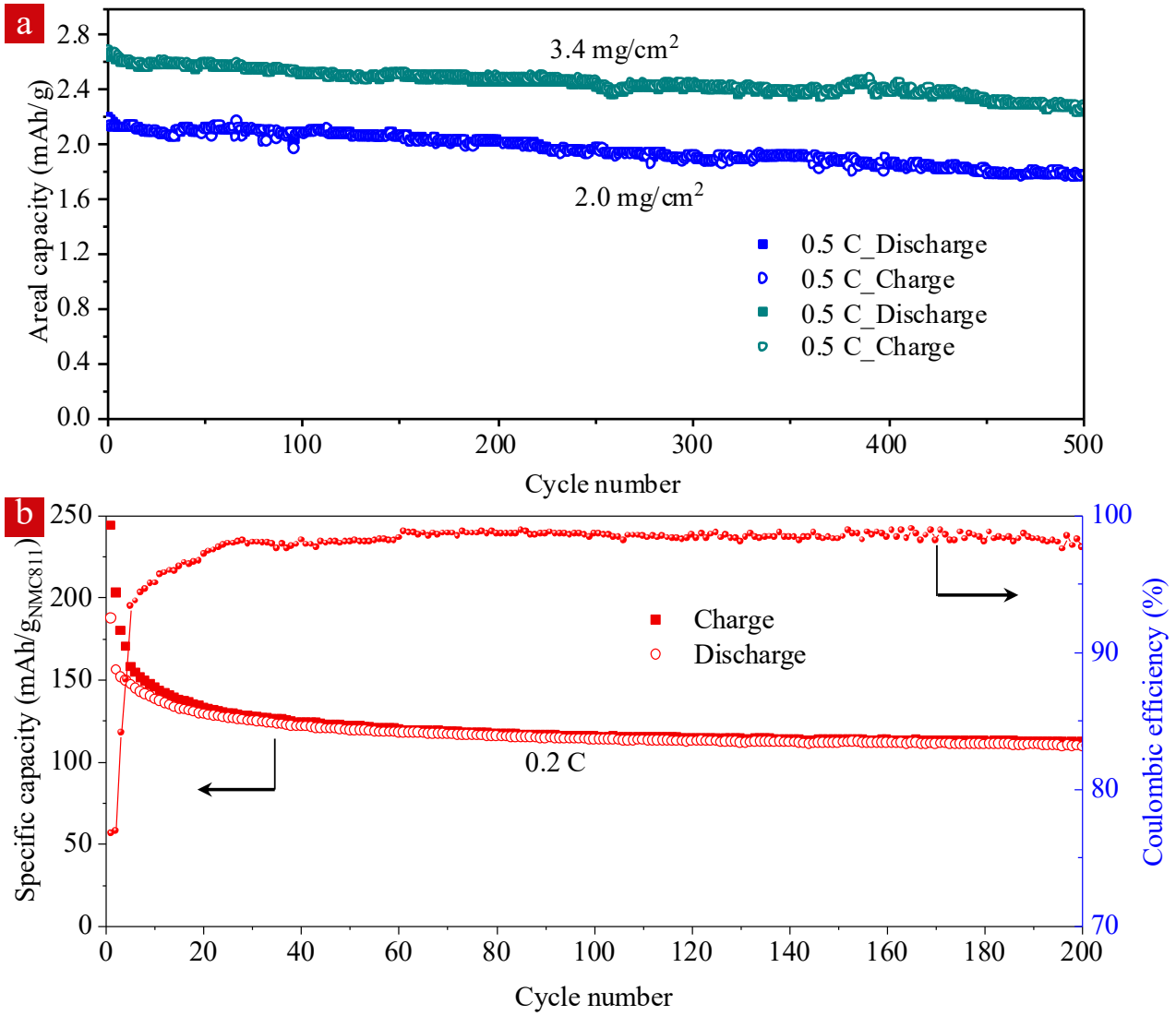

Figure S6. Battery cycling performance. (a) Areal capacity *vs* cycle number of the battery at 0.5 C. (b) Full cell cycling performance at 0.2 C. Specific capacity was calculated based on NMC811. The activation was done at 0.05 C for first 4 cycles.

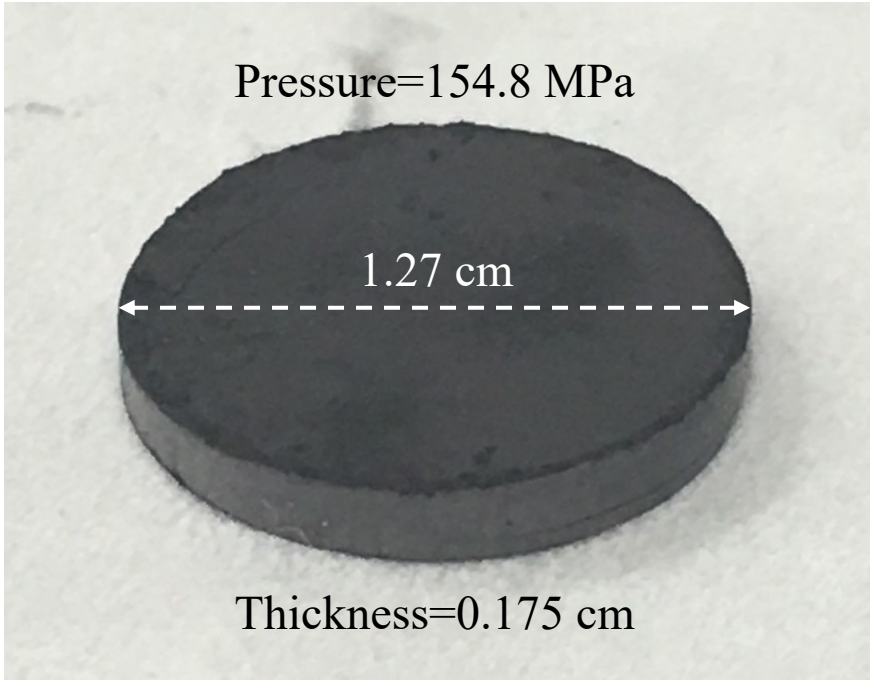

Figure S7. Density of the obtained GeO_x@MXene composite. The pellet with a diameter of 1.27 cm was made by using 0.5 g GeO_x@MXene under a pressure of 154.8 MPa *via* hydraulic press, which shows a density of 0.900 g/cm^3 vs GeO_x.

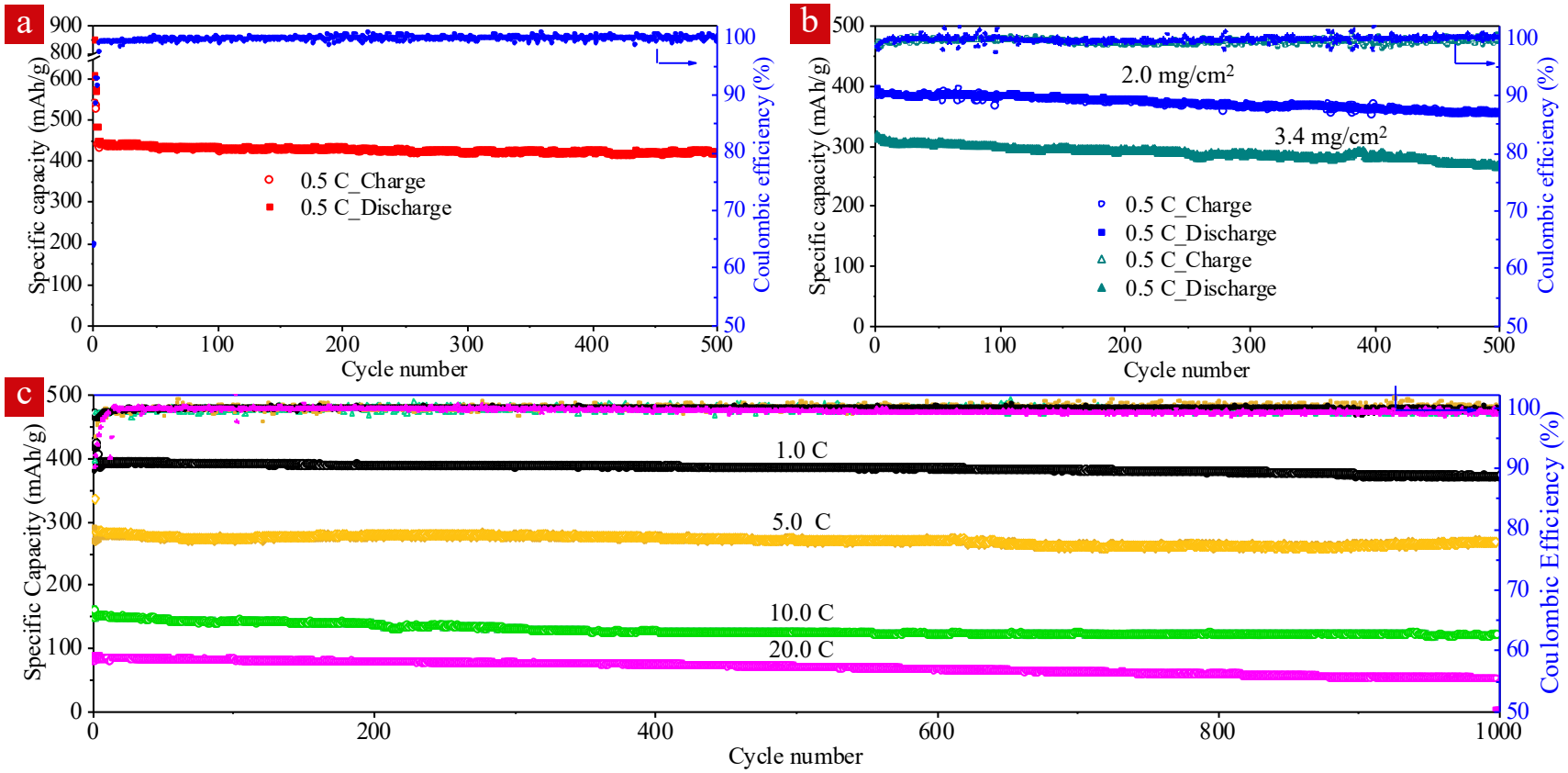

Figure S8. Battery cycling performance. Cycling performance of the battery with GeO_x@MXene as anode under (a) 0.5 C (first three cycles at 0.1 C for activation) and a loading of GeO_x of 1.0 mg/cm^2, (b) 0.5 C and GeO_x loadings of 2.0, 3.4 mg/cm^2, and (c) 1.0 C, 5.0 C,10.0 C and 20.0 C (1.0 mg/cm^2), respectively. The specific capacity was calculated based on the overall mass of GeO_x@MXene composite. All the coin cells were activated at 0.1 C for 3 cycles before cycling.

Table S1. Weight percentage calculation of GeO_x in GeO_x@MXene composite

Sample No.	Weight of MXene before synthesis (g)	Weight of GeO_x@MXene after synthesis (g)	GeO_x weight (%)
1	0.2600	0.4101	36.60
2	0.2602	0.4111	36.71
3	0.2605	0.4222	38.30
4	0.2601	0.4213	38.26
5	0.2601	0.4301	39.53
Average	-	-	37.9 wt%

Each sample was measured after drying at 60 ℃ in a vacuum oven for 12 h.

Table S2. XPS peak fitting results of Ge 3d in pure GeO_x

	Peak BE	FWHM eV	Area (P) CPS•eV	Atomic %
Ge	29.30	1.26	5351.39	11.72
Ge^{+}	30.10	1.44	7668.84	16.80
Ge^{2+}	31.10	1..42	11062.74	24.23
Ge^{3+}	32.00	1.46	10036.88	21.99
Ge^{4+}	32.60	1.71	11532.58	25.26

X in GeO_x is estimated to be 1.32.

Table S3. Comparison of coin cell battery performance with germanium oxide as anode

Materials	Synthesis method	Cycling performance				Rate performance			Loading (mg/cm^2)	Ref
		Specific capacity (mAh/g)	Cycle number	Current (A/g)	Areal capacity (mAh/cm^2)	Specific capacity (mAh/g)	Cycle number	Current (A/g)		
3D porous Ge-C composite	Wet chemical and carbonization	1598	100	0.16	~1.6	260	200	160 (100 C)	1-2	1
GeO_2 encapsulated Ge	Hydrothermal	1333.5	30	0.1	~0.59-0.83	665.3	100	0.5	0.44-0.62	2
Nanocrystalline GeO_2	PS template assisting	521	1000	0.3	~0.26-0.52	480	200	1	0.5-1	3
Ge/GeO_2/Carbon	Casting and high temperature carbonization	~1050	90	0.5	1.65	428	N/A	8	1-1.35	4
Vertically aligned graphene@amorphous GeO_x sandwich nanoflakes	Microwave plasma enhanced chemical vapor deposition	1008	100	~366 (C/3)	N/A	545	N/A	16.5(15 C)	N/A	5
GeO_x/Reduced graphene oxide	Wet chemical method	1600	N/A	0.1	N/A	410	N/A	20	N/A	6
GeO_x-coated reduced graphene oxide balls	Ultrasonic spray pyrolysis at 700 °C	758	700	2	~0.91	629	1600	5	~1.2	7
GeO_x@C core shell fiber	Coaxial electrospinning and high temperature carbonization	875	400	0.16	N/A	513	500	1.6	N/A	8
GeO_x/multi-walled CNT composite	Wet chemical method and spray dry	~1000	300	0.5	~0.52-1.22	365	N/A	10	0.52-1.22	9
Ge/GeO_2 ordered mesoporous carbon nanocomposite	Nanocasting and reduction by H_2	1018	100	0.1	N/A	395	100	2	N/A	10
GeO_x@MXene	Wet chemical method	1048.1	500	0.5 (0.5 C)	1.05	128.2	1000	24 (20C)	~1	**This work**
						300.5	1000	12 (10C)		
						671.6	1000	6 (5C)		
		886.0	500	0.5 C	1.77	N/A			2.0	
		671.7	500	0.5 C	2.28	N/A			3.4	

§. Areal capacity is estimated based on the loading and specific capacity.

Calculation of the theoretical capacity of GeO_x:

$$GeO_x + 2xLi \rightarrow Ge + xLi_2O. \quad (1)$$

$$Ge + 4.4Li \leftrightarrow Li_{4.4}Ge. \quad (2)$$

$$Q_{theoretical} = \frac{nF}{3600\ Mw} mAh/g$$

Where *n* is the number of charge carrier, *F* is the Faraday constant and *Mw* is the molecular weight of the active material (GeO_x) used in the electrode.
The theoretical capacity of GeO_x (X=1.57) was calculated as:

$$Q_{theoretical} = \frac{(4.4 + 2 * 1.57) * 96458 * 1000}{3600 * (72.63 + 16 * 1.57)} = 2066\ mAh/g$$

As the Equation 1 is not reversible, the reversible theoretical capacity of GeO_x was calculated as:

$$Q_{theoretical} = \frac{4.4 * 96458 * 1000}{3600 * (72.63 + 16 * 1.57)} = 1206\ mAh/g$$

Reference

1. Ngo, D. T.; Le, H. T. T.; Kim, C.; Lee, J. Y.; Fisher, J. G.; Kim, I. D.; Park, C. J. Mass-Scalable Synthesis of 3D Porous Germanium-Carbon Composite Particles as an Ultra-High Rate Anode for Lithium Ion Batteries. *Energy Environ. Sci.* **2015,** *8*, 3577-3588.
2. Yan, S. C.; Song, H. Z.; Lin, S. R.; Wu, H.; Shi, Y.; Yao, J. GeO_2 Encapsulated Ge Nanostructure with Enhanced Lithium-Storage Properties. *Adv. Funct. Mater.* **2019,** *29*, 1807946.
3. McNulty, D.; Geaney, H.; Buckley, D.; O'Dwyer, C. High Capacity Binder-Free Nanocrystalline GeO_2 Inverse Opal Anodes for Li-Ion Batteries with Long Cycle Life and Stable Cell Voltage. *Nano Energy* **2018,** *43*, 11-21.
4. Hwang, J.; Jo, C.; Kim, M. G.; Chun, J.; Lim, E.; Kim, S.; Jeong, S.; Kim, Y.; Lee, J. Mesoporous Ge/GeO_2/Carbon Lithium-Ion Battery Anodes with High Capacity and High Reversibility. *ACS Nano* **2015,** *9*, 5299-5309.
5. Jin, S. X.; Li, N.; Cui, H.; Wang, C. X. Growth of the Vertically Aligned Graphene@Amorphous GeO_x Sandwich Nanoflakes and Excellent Li Storage Properties. *Nano Energy* **2013,** *2*, 1128-1136.
6. Lv, D. P.; Gordin, M. L.; Yi, R.; Xu, T.; Song, J. X.; Jiang, Y. B.; Choi, D.; Wang, D. H. GeO_x/Reduced Graphene Oxide Composite as an Anode for Li-Ion Batteries: Enhanced Capacity *via* Reversible Utilization of Li_2O Along with Improved Rate Performance. *Adv. Funct. Mater.* **2014,** *24*, 1059-1066.
7. Choi, S. H.; Jung, K. Y.; Kang, Y. C. Amorphous GeO_x-Coated Reduced Graphene Oxide Balls with Sandwich Structure for Long-Life Lithium-Ion Batteries. *ACS Appl. Mater. Interfaces* **2015,** *7*, 13952-13959.
8. Li, M.; Zhou, D.; Song, W. L.; Li, X. G.; Fan, L. Z. Highly Stable GeO_x@C Core-Shell Fibrous Anodes for Improved Capacity in Lithium-Ion Batteries. *J. Mater. Chem. A* **2015,** *3*, 19907-19912.
9. He, W.; Tian, H. J.; Wang, X. L.; Xin, F. X.; Han, W. Q. Three-Dimensional Interconnected Network GeO_x/Multi-Walled CNT Composite Spheres as High-Performance Anodes for Lithium Ion Batteries. *J. Mater. Chem. A* **2015,** *3*, 19393-19401.
10. Zeng, L. X.; Huang, X. X.; Chen, X.; Zheng, C.; Qian, Q. R.; Chen, Q. H.; Wei, M. D. Ge/GeO_2-Ordered Mesoporous Carbon Nanocomposite for Rechargeable Lithium-Ion Batteries with a Long-Term Cycling Performance. *ACS Appl. Mater. Interfaces* **2016,** *8*, 232-239.